Simple Fabrication and Carrier Type Modification of Semi-Conductive C/Al_2O_3 Composites by Powder Mixtures and Pulsed Electric Current Sintering

Huu Hien Nguyen
Nagoya Institute of Technology
Yunzi Xin
Nagoya Institute of Technology
Takashi Shirai (shirai@nitech.ac.jp)
Nagoya Institute of Technology https://orcid.org/0000-0002-3438-6840

Research Article

Keywords: semi-conductive ceramic, carbon-alumina composite, pulsed electric current sintering, electrically conductive ceramic.

Posted Date: October 12th, 2021

DOI: https://doi.org/10.21203/rs.3.rs-960257/v1

Abstract

Semi-conductive C/Al_2O_3 ceramic composites were successfully fabricated by a pretty simple approach, combining a powder mixture process and pulsed electric current sintering. In order to obtain homogeneous distribution of carbon contents, popular polymers were used as carbon fillers to mix with Al_2O_3 powder by a wet ball milling step. The sintering was conducted by pulsed electric current sintering without any special requirement of the reductive environment like in conventional sintering. Density of bulk bodies, states of carbon contents after sintering and the electrical properties were analyzed in this study. Although the density of sintered bodies and their electrical properties were not superior, those characteristics of C/Al_2O_3 ceramic composites in this study were still comparatively high among semi-conductive ceramics. Especially, the carrier type of semi-conductive C/Al_2O_3 composites could be modified easily by adding polycarboxylic acid (PCA) in the powder mixture as a dispersant.

1. Introduction

In recent years, conductive ceramic composites have been developed gradually. The advantages of conductive ceramic composites over the conventional ceramic materials are not only the electrically functional properties but also the improvements in mechanical strength or heat resistance [1–6]. The conductive ceramic composites are noteworthy for applications of fuel cells, lithium-ion battery, electromagnetic shielding, thermal energy storage, etc. [7–11]. In order to fabricate conductive ceramic composites, the common system is the combination of ceramic materials, such as alumina, silica, zirconia, and various kinds of carbon fillers, such as graphene, graphene oxide, graphite, carbon nanotube (CNT) [1–5, 8, 9].

Although Al_2O_3 is the most widely used ceramic material, its functional applications are still severely limited due to its low toughness and poor electrical conductivity. One method to improve both mechanical and electrical properties of Al_2O_3 ceramics is reinforcing alumina with various carbon fillers, such as graphene or CNT [2–5, 12], which is conventionally mixed with Al_2O_3 powder via a milling process. Because graphene or CNT is easy to be aggregated, their homogeneous dispersion in pre-sintered powders as well as in sintered bodies is the major challenge for this composite material. The homogeneous dispersion of carbon fillers in ceramic matrix has been achieved by gel-casting method, followed by reductive sintering [13–16]. In this approach, Al_2O_3 powder was mixed with monomer, cross linker and dispersant, and the carbon fillers were dispersed homogeneously via the polymer network in the gel-casted green bodies. The graphitization occurred during the reductive sintering in Ar atmosphere. Although this approach significantly improved the homogeneity of carbon fillers in ceramic matrix, both carbon contents and reductive sintering conditions dramatically suppressed sintering behavior, which induced some difficulties to densify bulk bodies. In order to enlarge the potential applications for this composite material, increasing the density of sintered bodies is necessary. Pulsed electric current sintering techniques were also used to densify the C/Al_2O_3 ceramic composites in other studies [17, 18].

In this study, we conducted a remarkably simple route to fabricate semi-conductive C/Al_2O_3 ceramic composites. Polyvinyl alcohol solution (PVA), a common binder for ceramic materials, was used to mix with Al_2O_3 powder as a carbon filler. The sintering process was conducted by PECS, which improved the densification of C/Al_2O_3 composites in a shorter time duration without any environmental control. The importance of the homogeneous dispersion of carbon fillers was also pointed out clearly. The characteristic of carbon contents in sintered bodies as well as the electrcial conductivity and semi-conductive properties of sintered bodies were investigated. Noticeably, the carrier type in fabricated C/Al_2O_3 composites was changed from p-type to n-type very easily by an addition of a dispersant from starting mixture.

2. Materials And Methods

A commercial Al_2O_3 powder (AA-04, Sumitomo Chemical) was used as the starting material. In the A series of samples, Al_2O_3 powder was mixed with the commercial PVA solution (Celuna WF-804, Chukyo Yushi Co., Ltd). The concentration of PVA was at 10 wt% of Al_2O_3 powder. The mixture was ball milled with water at the solid loading of 20 vol% in 24 h, followed by freeze drying in 2 days. The dried powder was slightly ground by mortar and pestle to crash soft agglomerates before sintering by PECS. The powder was loaded into a graphite die/punches set with diameter of 25 mm and the sintering process was temperature-controlled by a pyrometer focused at a small hole on the outer surface of the die. The final sintering temperature were 1400 or 1500°C and a uniaxial pressure of 20 or 80 MPa was applied through the whole sintering cycle. The controlling of sintering temperature is shown in Fig. 1.

For the B series of samples, Al_2O_3 powder was mixed with 10 wt% PVA and 1 wt% PCA (Celuna D-305, Chukyo Yushi Co., Ltd). Ball milling and freeze drying were similar to the A series. After that, the dried powder was sintered via two different techniques: with and without grinding by mortar and pestle. Fig. 2 shows the different between ground powder and aggregated powder before sintering. The samples of B series were sintered by PECS with only one condition: 1400°C for 20 min.

After sintering, the samples were roughly polished both surfaces to remove residual carbon sheets. Density of samples was measured by both pycnometer and Archimedes method. The microstructure of samples was observed by a scanning electron microscope on the fractured surfaces of samples. Raman spectrum were analyzed on the cross-sectional surfaces of samples by a Raman spectroscopy with a 532-nm laser source. A piece of each sample was crashed into powder to measure the amount of carbon remained in the sintered bodies by a combustion-type carbon analyzer (LECO CS744).

Each sample was cut into a 4x8 mm^2 piece to measure the electrical conductivity by a physical property measurement system (PPMS, Quantum Design Inc.) at temperature ranging from 200 to 300K. The measurements of Hall resistivity were also conducted with the magnitude of magnetic field in the range of -1 to 1 T at several temperatures from 200 to 300 K. Carrier density and mobility are calculated from the measured values of electrical conductivity and Hall resistivity.

Bonding states of carbon contents in various samples were analyzed by an X-ray photoelectron spectroscopy (XPS, M-probe, SSI, USA) with Al K_{α} source.

A small amount of Al_2O_3 powder was mixed with PCA and PVA following the concentration of A-series (10 wt% PVA) and B-series (10 wt% PVA and 1 wt% PCA) powders in de-ionized water at low solid loading for the measurements of absorption of organic carbon. The two slurries were well shaken at speed of 150 rpm, followed by a centrifugation at 15000 rpm for 20 min to separate the solid parts. The total amount of organic carbon in supernatants was measured by a total organic carbon analyzer (TOC-L, Shimadzu), and the amount of organic substances adsorbed on Al_2O_3 powder surfaces was calculated from TOC results.

3. Results & Discussion

3.1. Density, porosity, microstructure and total amount of carbon of sintered samples:

Table 1 shows the notations and density of sintered samples. The LECO results indicating the amount of residual carbon inside sintered bodies are showed in Table 1. The theoretical density of each sample was calculated from LECO results, assuming the theoretical densities of alumina and graphite were 3.99 and 2.25 g/cm^3 correspondingly. The relative density and open porosity were calculated from the results of Archimedes method and calculated theoretical density. Closed porosity is calculated from results of pycnometer. Relative density, open porosity and closed porosity are also showed in Table 1. The typical sintering behavior was pointed out clearly. Density of sintered bodies tends to be increased with increasing of sintering temperature or applied pressure.

Table 1
Residual carbon content, density and porosity of sintered C-Al_2O_3 samples:

Sample	Conditions	Residual carbon *(wt%/vol%)*	Theoretical density *(g/cm^3)*	Relative density *(%)*	Open porosity *(%)*	Closed porosity *(%)*
A-1	PVA10 1400°C - 20 MPa	0.80 / 1.41	3.965	89.1	9.7	0.14
A-2	PVA10 1400°C - 80 MPa	0.53 / 0.94	3.974	98.5	0	1.64
A-3	PVA10 1500°C - 20 MPa	0.52 / 0.92	3.974	97.2	0.1	2.69
A-4	PVA10 1500°C - 80 MPa	0.45 / 0.80	3.976	98.1	0	1.43
B-1	PVA10.PCA1 1400°C - 20MPa	1.05 / 1.85	3.958	87.6	10.2	0.35
B-2	PVA10.PCA1 1400°C - 20MPa Aggre. powder	1.08 / 1.90	3.957	84.7	12.3	0.57

Despite of the same sintering conditions, relative density of sample B-1 was lower than that of sample A-1. From TOC results, the absorption of organic carbon on the surfaces of Al_2O_3 powder was enhanced by the addition of PCA, from 0.6 wt% in the A-series powders to 5 wt% in the B-series powders. With the higher amount of organic carbon absorbed on the Al_2O_3 surfaces, the residual carbon within sintered body of sample B-1 was also higher, which suppressed more the densification during sintering. In comparison with sample B-1, sample B-2 had even lower relative density, despite of the comparative amount of remaining carbon contents (1.05 and 1.08 wt% correspondingly). It was attributed to the aggregation of the pre-sintered powder. In order to preserve the polymer network in powder, sample B-2 was sintered from as-aggregated powder after drying. As a consequence, the powder was not packed perfectly in the die and generated high porosity from the original aggregates.

The microstructure of all sintered samples is shown in Fig. 3. A slight grain growth was only observed in sample A-4, which was sintered at high temperature and high pressure. All of the other sintered samples showed comparative grain size. It was obvious that the influence of carbon impurity strongly suppressed the grain growth of Al_2O_3 samples. The increasing in sintering temperature from 1400°C to 1500°C (samples A-1 and A-3) or the increasing in uniaxial pressure from 20 MPa to 80 MPa (samples A-1 and A-2) distributed only to the densification and significantly increased the relative density of sintered

samples. From SEM images, samples B-1 and B-2 showed a clearly lower relative density in comparison to other samples.

3.2. Raman results:

Figure 4 shows the Raman spectra investigated on the cross-sectional surfaces of sintered bodies and Fig. 5 demonstrates the ratios I_D/I_G and $I_{G'}/I_G$ of Raman peaks. All Raman spectra were normalized by the intensity of G peak. The three obvious peaks of graphite structure are assigned for D band (1350 cm^{-1}), G band (1590 cm^{-1}) and G' band (2695 cm^{-1}) [15, 19, 20]. In comparison among samples of A series, the graphite structure was generated more with increasing of sintering temperature or applied pressure during PECS process. The shoulder peak next to G-band at about 1625 cm-1, indicating the structure of graphite-like carbon, had slightly lower intensity when the sintering temperature increased from 1400°C to 1500°C. This shoulder peak was much weaker when the applied pressure in PECS increase from 20 MPa to 80 MPa. From Raman results, the graphitization of carbon was obviously promoted at higher sintering temperature and higher pressure. The amount of layers in graphite structure, which is indicated by intensity of G'-band, also increased at higher temperature and pressure. In comparison with the graphitization in pressureless sintering methods reported in previous works [14, 15], PECS has advantages to the formation of graphite structure. The graphite structure in C/Al_2O_3 composite sintered at 1500°C and 80 MPa is similar to the pressureless-sintered sample at 1600°C [15]. By the influences of applied pressure in PECS, the ratio of graphite structure tends to be promoted. As discussed above, the graphitization was promoted with higher applied pressure. However, the total amount of carbon remained inside sintered samples was lower than other studies with pressureless sintering. Even with the original concentration of PVA at 10 wt% in comparison with Al_2O_3 powder, the remained carbon content in sintered bodies was in the range of 0.5-1 wt%, which was only about 10% of the original carbon content in PVA. The amount of remaining carbon inside sintered samples reduced with increments of sintering temperature or pressure. The results seem to be obvious because the oxidization and vaporization of carbon contents may be enhanced by higher temperature or pressure.

3.3. Electrical conductivity and semi-conductive properties:

Electrical conductivity of C/Al_2O_3 sintered bodies with different sintering conditions is showed in Fig. 6. In all cases, the electrical conductivity of C/Al_2O_3 composites increased as the temperature increased, indicating that C/Al_2O_3 composites fabricated by PECS in our study exhibited semi-conductive properties. The highest electrical conductivity in A-series samples at ambient temperature is nearly 0.9 S/cm, which value belongs to the sample sintered at 1400°C and 20 MPa. Despite of the smallest content of graphite as well as fewest layers of graphite structure among sintered samples, sample A-1, sintered at 1400°C and 20 MPa, had the highest electrical conductivity. One of the possible reasons of its highest electrical conductivity is its highest residual carbon amount as well as its lowest relative density. Menchavez et al. reported that electrical conductivity of C/Al_2O_3 composites increased while the bulk density of sintered sample decreased [13]. Reason of this relationship was reported as the larger amount of carbon filler adding to C/Al_2O_3 composites, which resulted to both the promotion of electrical conductivity and the

reduction of bulk density due to the suppression of sintering ability. In this study, the remaining amount of carbon in sample A-1 was the most among A-series samples. Although the overall graphitization in other A-series samples were increased by higher temperature or/and higher applied pressure, their electrical conductivity was still much lower than sample A-1. Our conjecture is that the increase of sintering temperature and pressure not only promoted the graphitization degree but also pushed more carbon substances out of the bulk bodies. Consequently, the amount of residual carbon contents in bulk samples reduced with increasing of sintering temperature or pressure. More importantly, at high temperature and pressure, the densification as well as the removal of carbon substances were dramatically accelerated, which possibly eliminated many conductive paths of graphite at the grain boundaries. As a result, a good graphite structure with many stacking layers might be formed inside bulk samples but not connected well each other along grain boundaries in the ceramic matrix. Therefore, although the Raman results indicated the higher graphitization degree with more stacks of graphite layers in samples A-2 or A-4, their conductivity was much lower than that of sample A-1.

Comparing among three sample A-1, B-1 and B-2, the electrical conductivity of B-series samples was 3-4 times higher than sample A-1, even though they were sintered at the same sintering condition. The results of electrical conductivity of B-series samples illustrated that the structure of polymer network in pre-sintered powder strongly affected to the graphitization process as well as the graphite structure in sintered bodies and their electrical conductivity. With the addition of PCA as a dispersant, the carbon fillers in the ball-milled slurries were expected to be dispersed more homogeneously, which led to a homogeneous distribution of carbon contents in the sintered bodies. Especially, by packing the aggregated powder directly into the graphite die of PECS, sample B-2 obtained the highest electrical conductivity. This result is consistent with the results on the graphite structure of sample B-2 in comparison to sample A-1 or B-1. The high ratio of graphite content as well as large amount of stacking layers of graphite led to the high electrical conductivity of sample B-2.

The Hall resistivity measurements were conducted with samples A-1, B-1 and B-2. Hall effect could not be observed clearly with the other 3 sample due to the low electrical conductivity and discontinuous graphite structure. The dependence of Hall resistivity of samples A-1, B-1 and B-2 on intensity of magnetic field at different temperature is showed in Fig. 7. While the Hall resistivity of samples B-1 and B-2 is linearly related to the intensity of magnetic field, the points in the graphs belongs to samples A-1 at all temperature are scattered too much. The reason for the scattered values might be the heterogeneous distribution of graphite structure in the sintered bodies. Because the pre-sintered powders were simply mixed with PVA by wet ball milling, the distribution of PVA in the synthesized powders might not be homogeneously optimized. Otherwise, the actual distribution of temperature and pressure during PECS, which cannot be investigated directly, may cause the heterogeneous distribution of graphite structure in sintered bodies. For the B-series samples, the existence of PCA as a dispersant made Al_2O_3 powder and PVA dispersed well in the slurry, leading to the better polymer network as well as homogeneous distribution of graphite in the sintered bodies.

The results of Hall resistivity also showed that sample A-1 contains positive-charged carriers while samples B-1 and B-2 have negative-charged ones. The modification between n-type and p-type in graphene/Al_2O_3 composites has been reported by Fan et al. [21]. Although the graphene/Al_2O_3 composites intrinsically contain negative-charged carriers, the positive charges are assumably introduced by the doping from the Al_2O_3 matrix or by the point defects in graphite structure which can be considered as the electron acceptors [15, 16, 21]. In the other words, C/Al_2O_3 composites may contain both intrinsic negative-charged electrons within the graphite structure and conceivably positive-charged holes at the contacting layers between graphite and Al_2O_3 grains. At the low concentration of graphite, the amount of positive charges possibly overwhelms and produce p-type semi-conductive properties. Otherwise, at high enough concentration of graphite, the amount of electron within graphite structure overcomes and the composites perform as n-type. In this study, by the additional of PCA, the surfaces of Al_2O_3 particles could adsorbed more organic carbon substances, that was confirmed by TOC results above. Hence, the residual amount of graphite in sintered bodies of B-1 and B-2 was higher than that in sample A-1. This is apparently same phenomena described by Fan et al. [21], so that A-1 samples showed p-type semi-conductive properties with lower concentration of graphite while B-1 and B-2 samples performed as n-type semi-conductive composites with higher concentration of graphite.

Figure 8 shows the carrier density and mobility of three samples A-1, B-1 and B-2. In all three samples, the relationship between Hall coefficient and the measuring temperature was not evident. The carrier density and the carrier mobility of sample A-1 were in the ranges of 0.8-3.8 × 10^{24} m^{-3} and 0.14-0.65 × 10^{-3} m^2/Vs correspondingly. In disregard of the sign (+/-) of the results, the carrier mobility of B-1 and B-2 samples were about 10 times higher than that of sample A-1. The improvement in carrier mobility in B-series samples may attributed to the distribution of carbon fillers in pre-sintered powder as well as the homogeneous graphite structure in the sintered bodies.

3.4. XPS results:

The interaction of carbon contents and Al_2O_3 surface in sintered samples was inspected by XPS results. Fig. 9a, 9b and 9c show the XPS spectra of C1s of 3 sintered samples A-1, B-1 and B-2 correspondingly. The peak fitting for all samples pointed out 5 peaks at around 282.2, 283.5, 284.3, 285.8 and 288.1 eV, distributing to C-Al, C-O-Al, C=C, C-C and C=O bindings [16, 22–26]. The differences in carrier types of the 3 samples are possibly explained by the differences in C-Al and C-O-Al bindings. Fig. 10 shows the ratio of each peak area over the total peak area in the 3 samples. The graph in Fig. 10 illustrated the decrease of C-Al bindings from sample A-1 to B-1 and B-2. In contrast, amount of C-O-Al bindings increased in the same order of 3 sample. The amount of C-Al bindings in sample A-1 from XPS results proved that the positive-charged carriers derived from the doping effect of Al atoms in graphite structure. In samples B-1 and B-2, with the addition of PCA, the absorption of carbon fillers on surface of Al_2O_3 powder seem to be stronger. Therefore, more C-O-Al bindings were created from the connections between carbon fillers and Al_2O_3 surface. The C-O-Al bindings tent to remain after sintering process and prevented the doping of Al atoms to graphite structure, that could be confirmed by the reduction of C-Al peak's area in samples B-1

and B-2. Moreover, residual amount of carbon in samples B-1 and B-2 is higher, leading to the higher stacking of graphene layers and giving B-series samples more negative-charged carriers than positive-charged ones. Besides the results in C-O-Al and C-Al bindings, the higher peaks of C=O bindings at around 288 eV in samples B-1 and B-2 also indicated that the polymer structures formed in B-series samples were more stable than in sample A-1. Hence, after sintering, both C=O and C-O-Al bindings remained more in B-series samples.

4. Conclusions & Remarks

Highly electrical conductivity C/Al_2O_3 ceramics were successfully fabricated by a very simple route, including a wet mixing of Al_2O_3 powder with polymers as carbon fillers and a sintering process by PECS. Although only PVA and PCA, a common binder and a common dispersant for ceramic materials, were used in this study, the electrical conductivity as well as the semi-conductive properties of the C/Al_2O_3 ceramics were quite high. The carrier charge type of C/Al_2O_3 composites can be controlled by the addition of PCA. In the future, both electrical and semi-conductive properties of C/Al_2O_3 ceramics fabricated by this route can be improved by controlling the polymer network in the pre-sintered powder, leading to a better distribution of graphite contents in sintered bodies.

A remark should be noticed in this study is that there is a trade-off between the density of sintered bodies and its electrical conductivity. The fabrication of C/Al_2O_3 semi-conductive ceramics by mixing Al_2O_3 powder with organic carbon fillers causes a certain difficulty in densification during sintering stage due to the carbon impurity and its homogeneous distribution. Consequently, with higher amount and better homogeneity of carbon content, the sintered bodies have low density and low mechanical strength but high electrical conductivity. Therefore, depending on actual applications, there should be a balance between mechanical and electrical properties.

References

1. Tatami J, Katashima T, Komeya K, et al. Electrical conductive CNT-dispersed silicon nitride ceramics. J Am Ceram Soc. 2005;**88**[10]:2889–93.
2. Mudra E, Hrubovcakova M, Shepa I, et al. Processing and characterization of fiber-reinforced and layered alumina-graphene composites. J Euro Ceram Soc. 2020;40:4808–17.
3. Ahmad K, Pan W, Qu Z. Multifunctional properties of alumina composites reinforced by a hybrid filler. Int J Appl Ceram Technol. 2009;**6**[1]:80–8.
4. Ahmad K, Pan W, Shi SL. Electrical conductivity and dielectric properties of multiwalled carbon nanotube and alumina composites. Appl Phys Lett. 2006;89:133122.
5. Michalek M, Sedlacek J, Parchoviansky M, et al. Mechanical properties and electrical conductivity of alumina/MWCNT and alumina/zirconia/MWCNT composites. Ceram Inter. 2014;40:1289–95.

6. Goor GVD, Sagesser P, Berroth K. Electrically conductive ceramic composites. Solid State Ionics. 1997;101-103:1163–70.
7. Hayfield PCS. Towards an electrically conductive ceramic. In: *Development of a New Material: Monolithic Ti_4O_7 Ebonex Ceramic*. The Royal Society of Chemistry; 2001. pp. 1–8.
8. Wu P, Lv H, Peng T, et al. Nano conductive ceramic wedged graphene composites as highly efficient metal supports for oxygen reduction. Sci Rep. 2014;4:3968.
9. Zhou M, Lin T, Huang F, et al. Highly conductive porous graphene/ceramic composites for heat transfer and thermal energy storage. Adv Funct Mater. 2013;23:2263–9.
10. Oskam G, Searson PC. Sol-gel synthesis and characterization of carbon/ceramic composite electrodes. J Phys Chem B. 1998;102:2464–8.
11. Bondar AM, Iordache I. Carbon/ceramic composites designed for electrical application. J Optoelect Adv Mater. 2006;**8**[2]:631–7.
12. Samoilov VM, Danilov EA, Nikolaeva AV, et al. Electrical conductivity of a carbon reinforced alumina resistive composite material based on synthetic graphite and graphene. Inorg Mater. 2018;**54**[6]:601–9.
13. Menchavez RL, Fuji M, Shirai T, Kumazawa T. Electricaly conductive porous alumina/graphite composite synthesized by starch consolidation with reductive sintering. J Euro Ceram Soc. 2014;34:717–29.
14. Kato T, Shirai T, Watanabe H, et al. Electricaly conductive properties of dense alumina/nano-carbon network composite fabricated by combination of gelcasting and argon sintering. Trans Mater Res Soc. 2009;**34**[3]:537–9.
15. Xin Y, Kumazawa T, Fuji M, Shirai T. High hole mobility of a semi-conductive alumina/nano-carbon ceramic composite fabricated by gel-casting and reductive sintering. J Euro Ceram Soc. 2019;39:1730–4.
16. Xin Y, Takeuchi Y, Hattori M, Shirai T. Enhanced electrical conductivity of alumina/nano-carbon ceramic composite via iodine impregnation of gel-casted alumina body and reductive sintering. J Euro Ceram Soc. 2019;39:4440–4.
17. Hirota K, Kasahara K, Kato M. Fabrication of dense composite utilizing pulsed electric current and pressure. J Soc Mater Sci Jpn. 2018;**67**[5]:539–44.
18. Saheb N, Hayat U, Hassan SF. Recent advances and future prospect in spark plasma sintered alumina hybrid nanocomposites. Nanomater. 2019;9:1607.
19. Bokobza L, Bruneel JL, Couzi M. Raman spectroscopic investigation of carbon-based materials and their composites - Comparison between carbon nanotubes and carbon black. Chem Phys Lett. 2013;590:153–9.
20. Aramesh M, Tran PA, Ostrikov K, Prawer S. Conformal nanocarbon coating of alumina nanocrystals for biosensing and bioimaging. J Carbon. 2017;122:422–7.

21. Fan Y, Jiang W, Kawasaki A. Highly conductive few-layer graphene/Al_2O_3 nanocomposites with tunable charge carrier type. Adv Funct Mater. 2012;22:3882–9.
22. Cueff R, Baud G, Benmalek M, et al. Alumina coatings on polyethylene terephthalate: characterisation and X-ray photoelectron spectroscopy study. Surf Coat Technol. 1996;80:96–9.
23. Hinnen C, Imbert D, Siffre JM, Marcus P. An in situ XPS study of sputter-deposited aluminum thin films on graphite. Appl Surf Sci. 1994;78:219–31.
24. Jankovsky O, Lojka M, Jirickova A, et al. Carbon-bonded alumina filters coated by graphene oxide for water treatment. Mater. 2020;13:2006.
25. Liu FC, Dong P, Lu W, Sun K. On formation of Al-O-C bonds at aluminum/polyamide joint interface. Appl Surf Sci. 2019;466:202–9.
26. Massaro C, Le QT, Pireaux JJ. XPS/AFM study of thermally evaporated aluminum/polycarbonate interface. Surf Interf Analys. 1994;21:425–9.

Figures

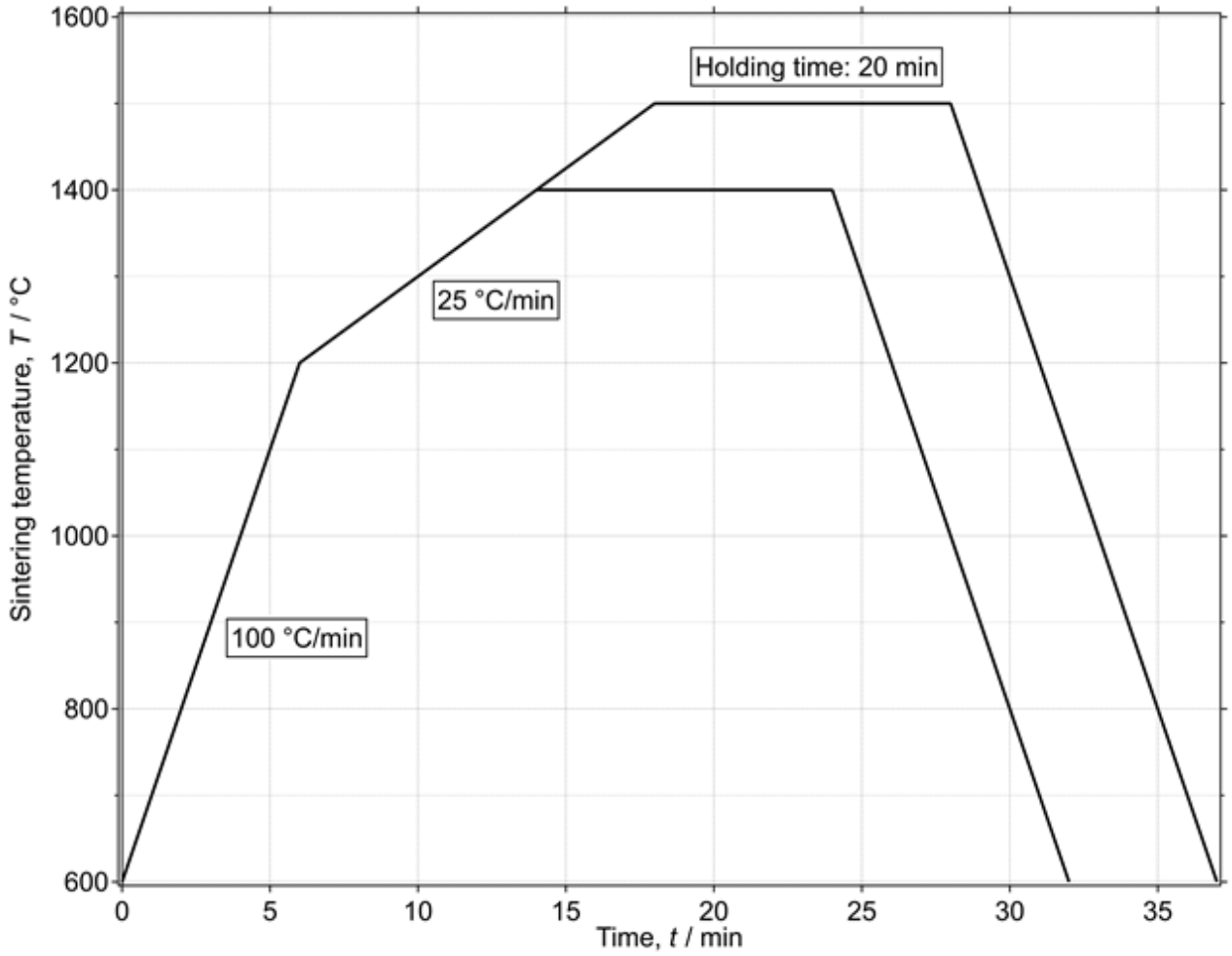

Figure 1

Temperature controlling program for PECS processes.

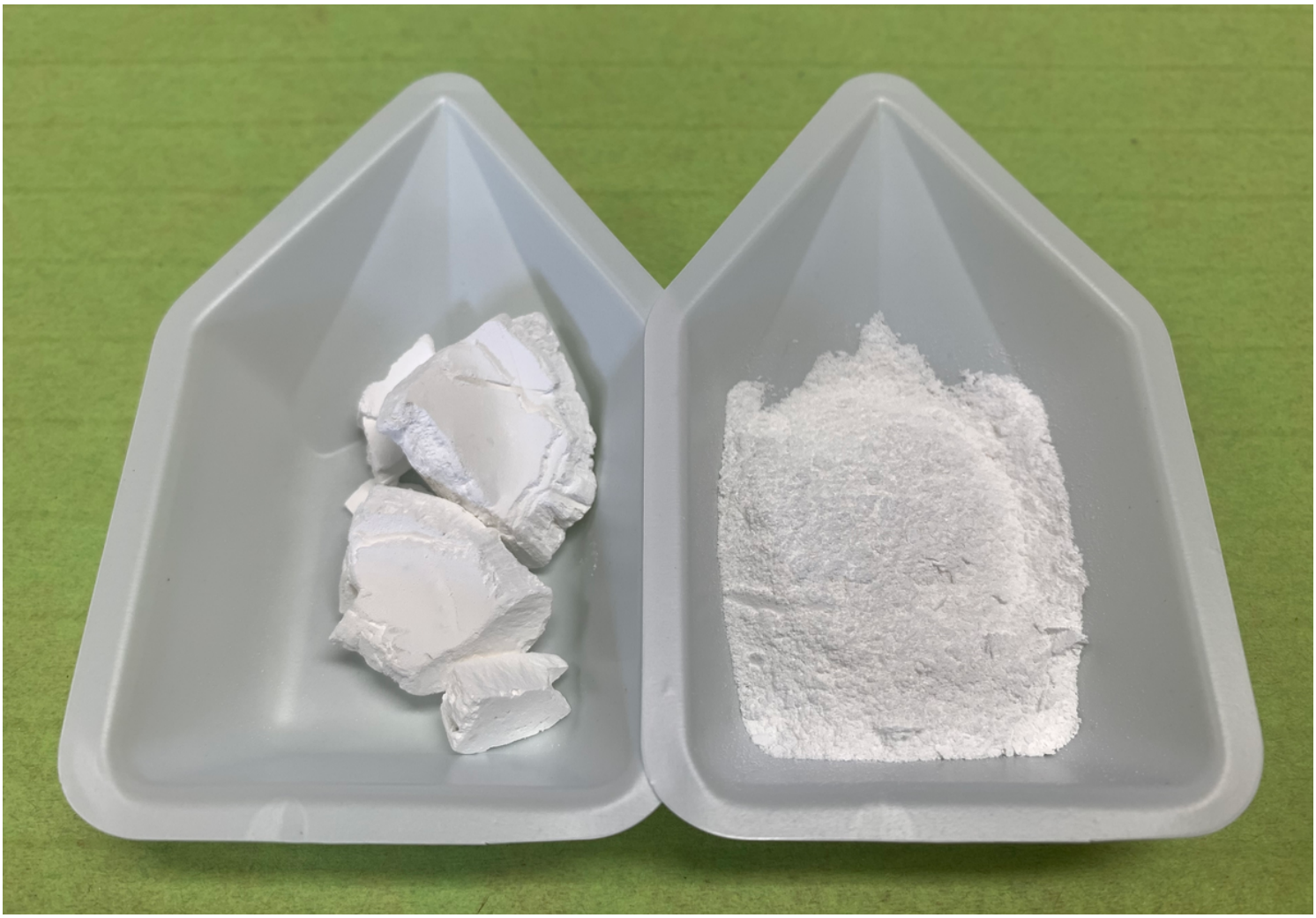

Figure 2

Aggregated powder (left) and crashed powder (right).

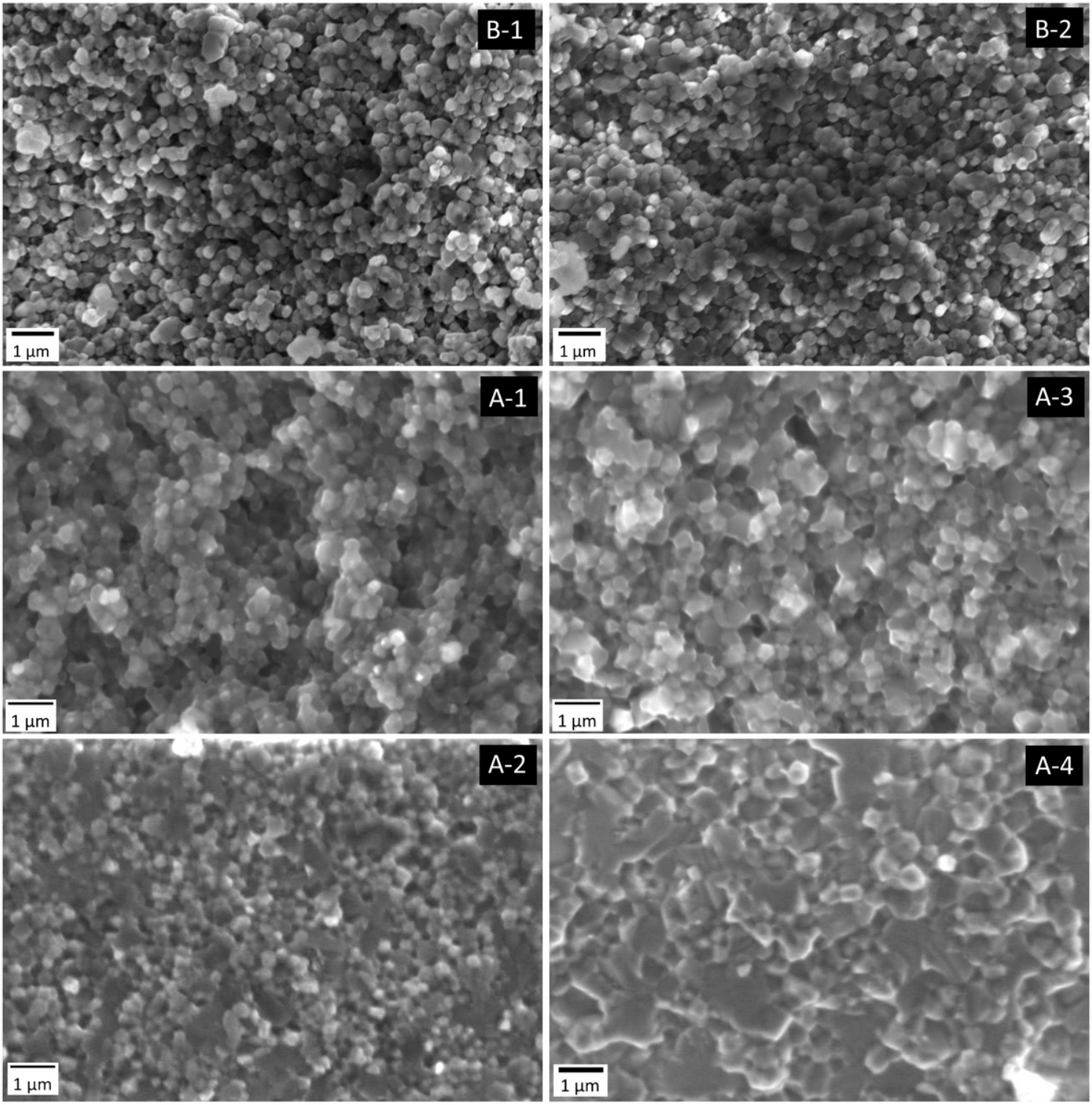

Figure 3

Microstructure of sintered samples.

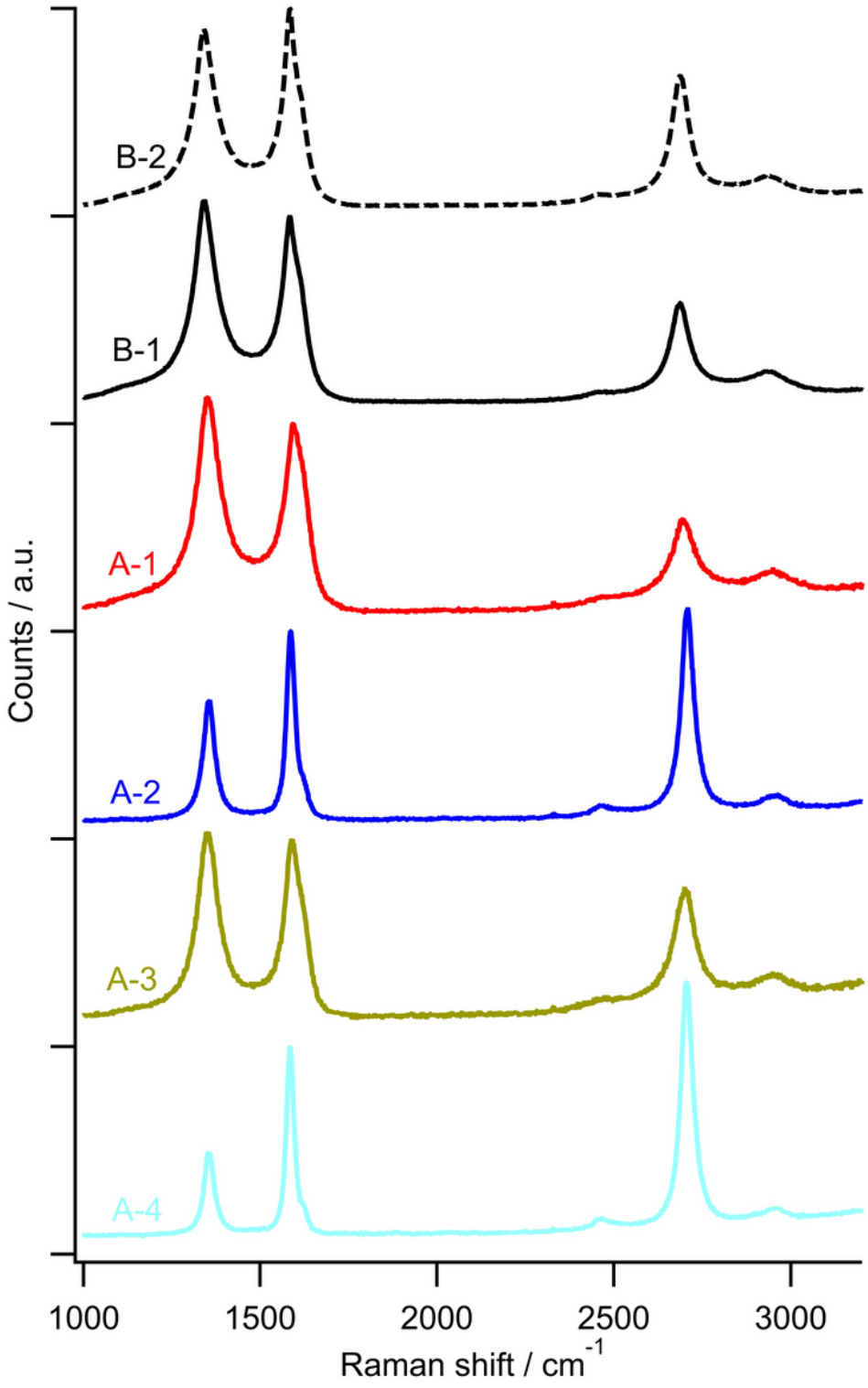

Figure 4

Raman spectrum of sintered C-Al2O3 samples

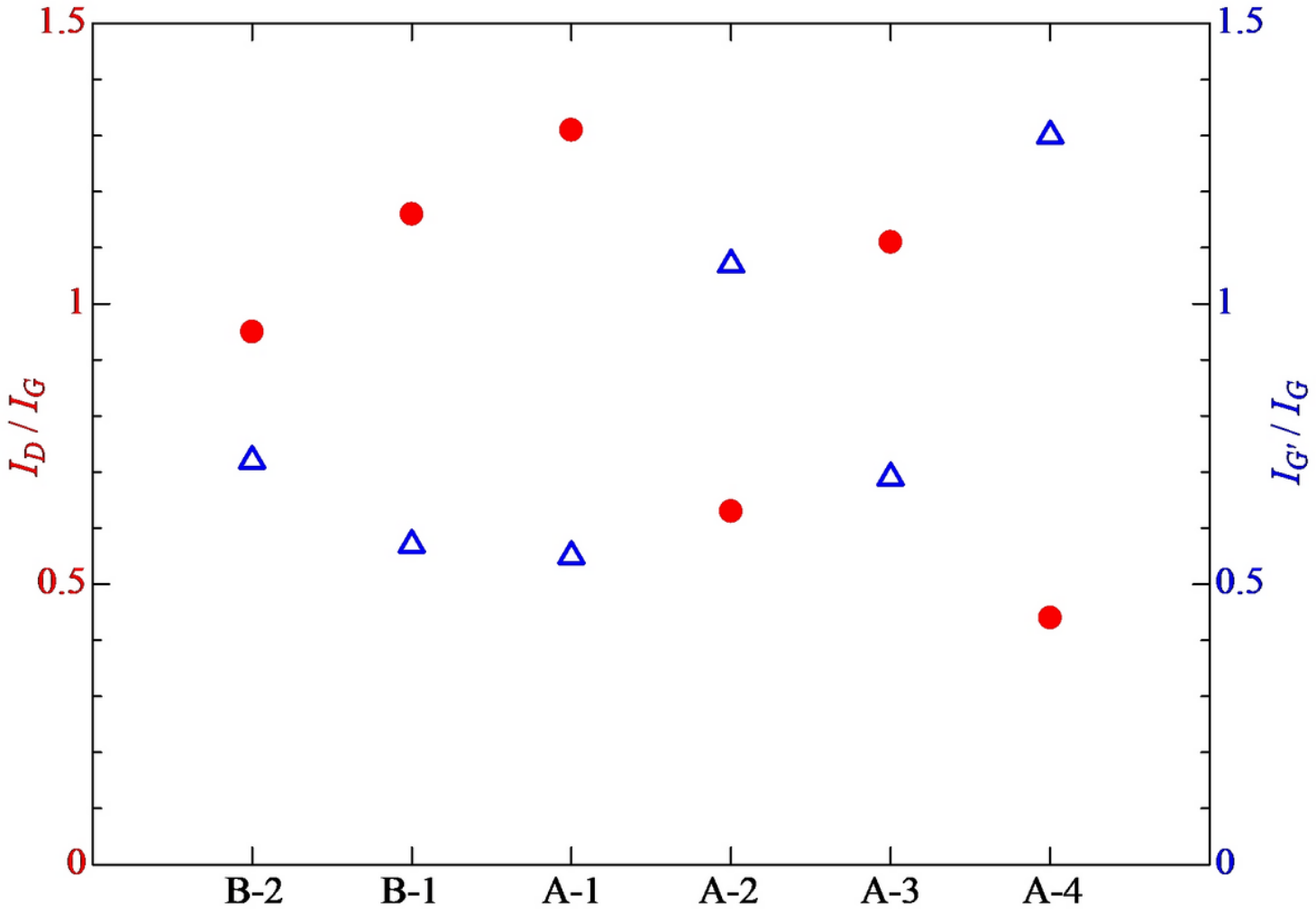

Figure 5

Intensity ratio of Raman peaks

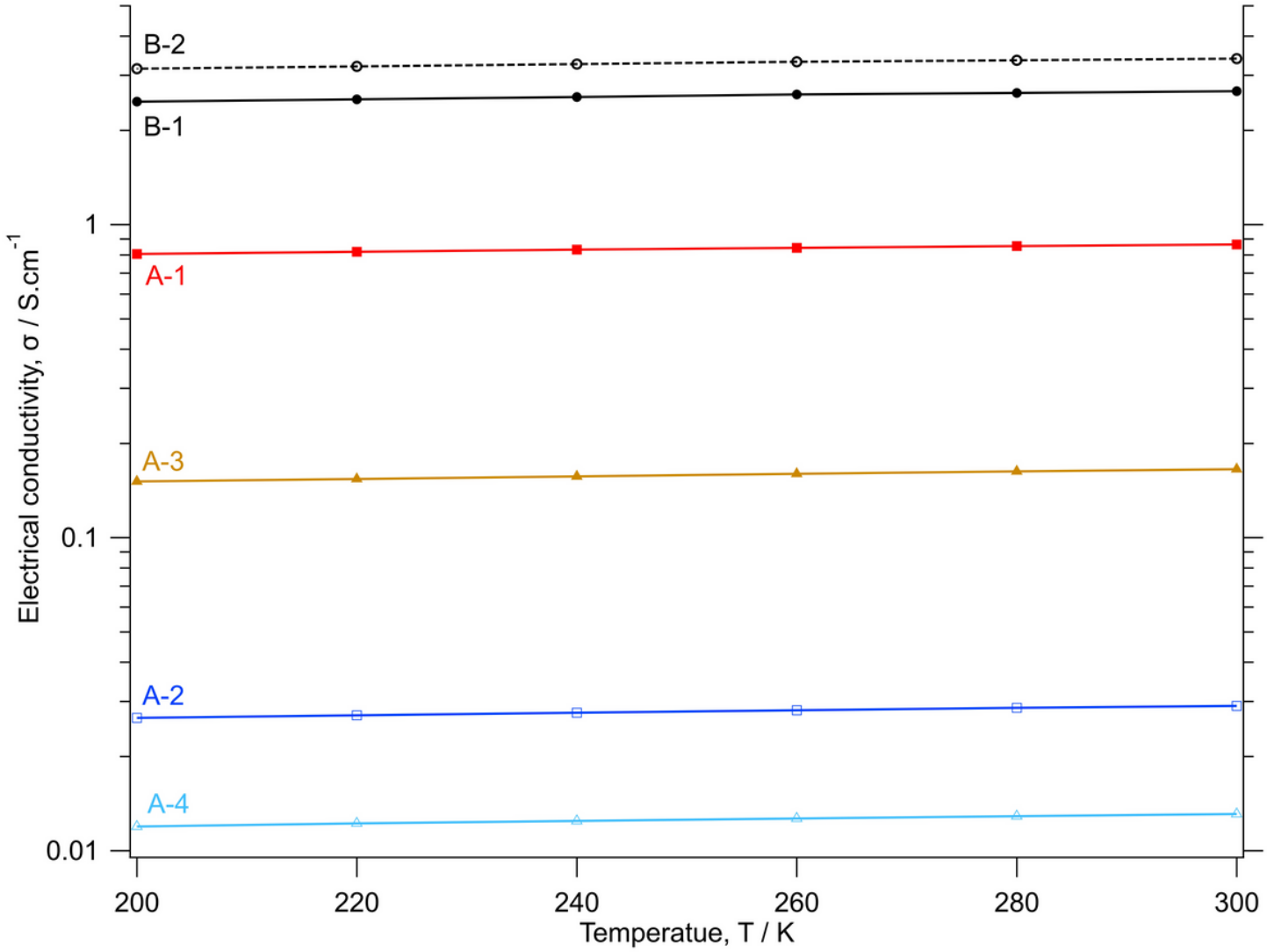

Figure 6

Electrical conductivity of sintered C-Al2O3 samples

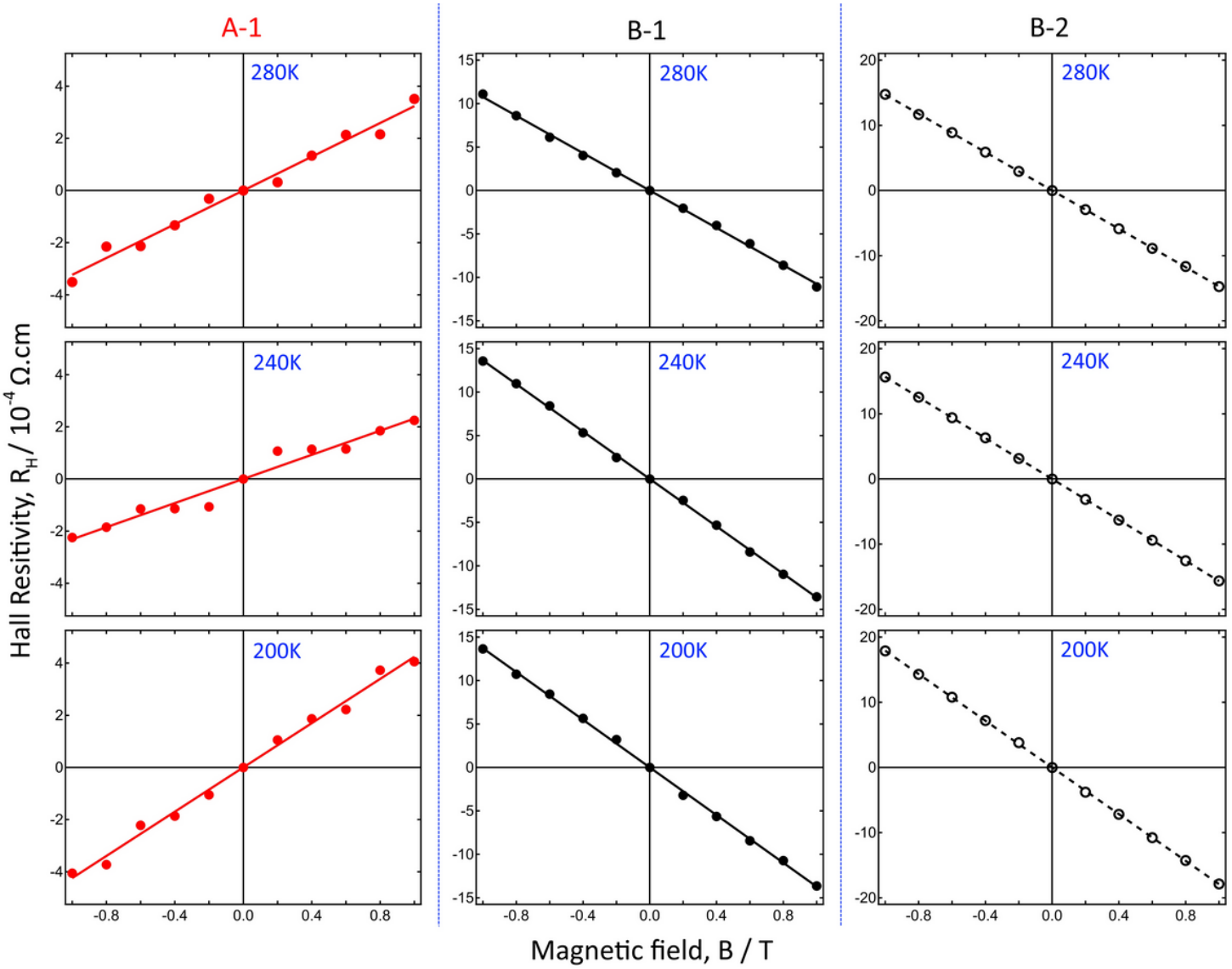

Figure 7

Dependence of Hall resistivity of samples A-1, B-1 and B-2 on magnitude of magnetic field at 280K, 240K and 200K

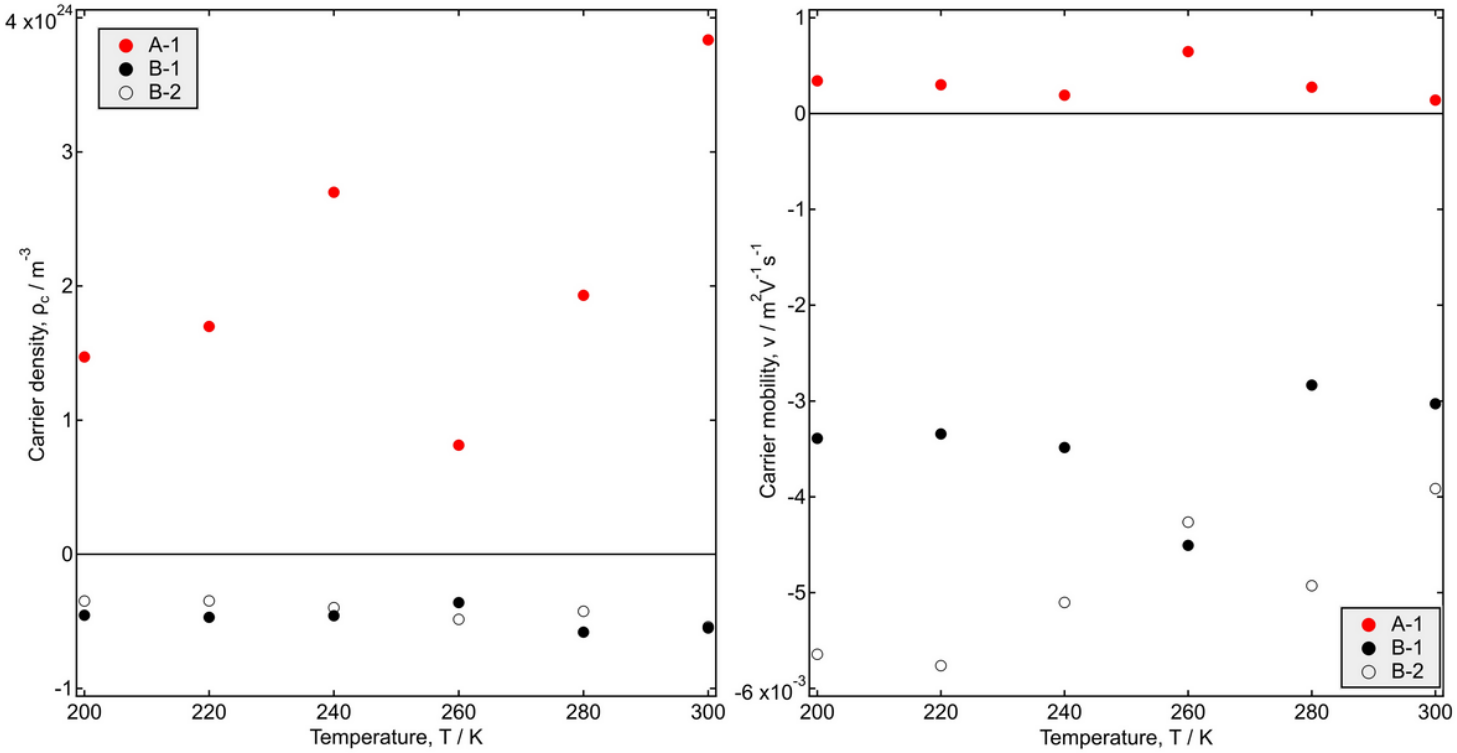

Figure 8

Carrier density and mobility of three samples A-1, B-1 and B-2.

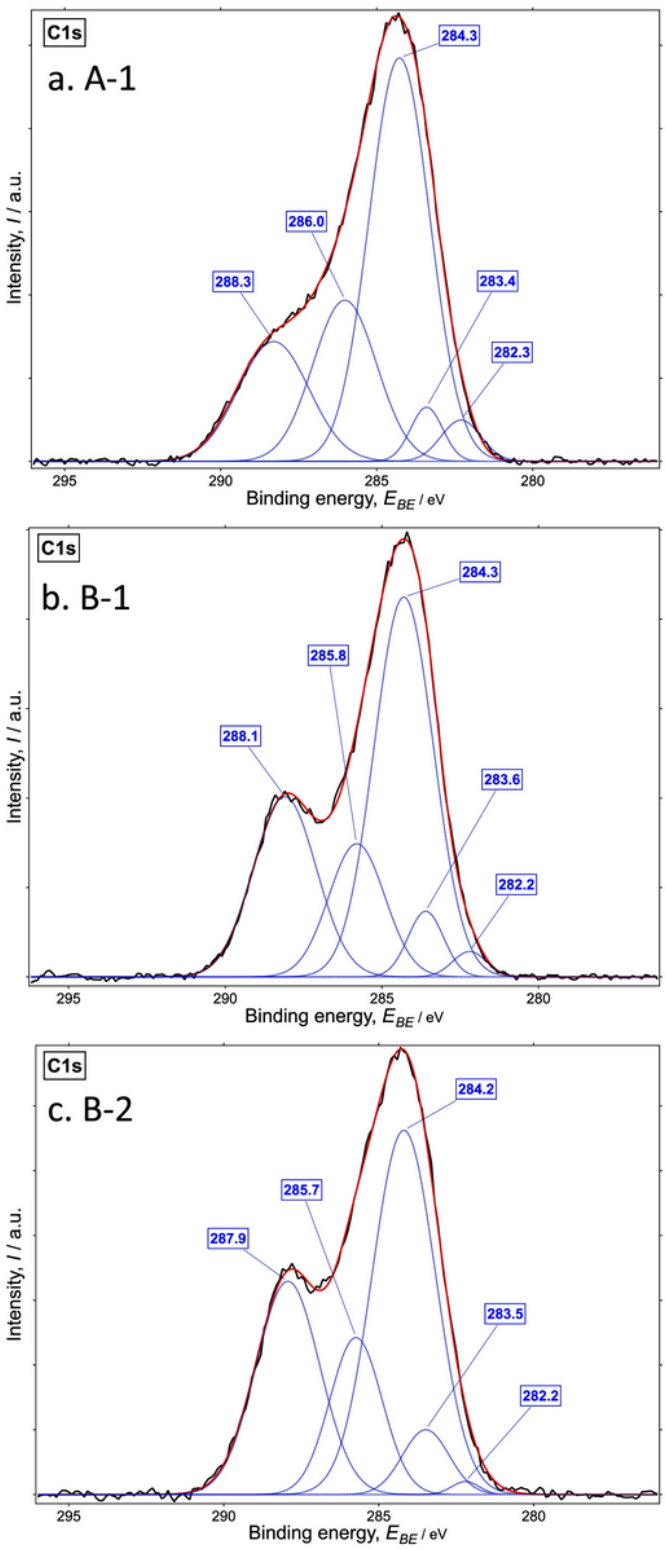

Figure 9

XPS results of C1s orbital of (a) A-1, (b) B-1 and (c) B-2 samples with peak fitting.

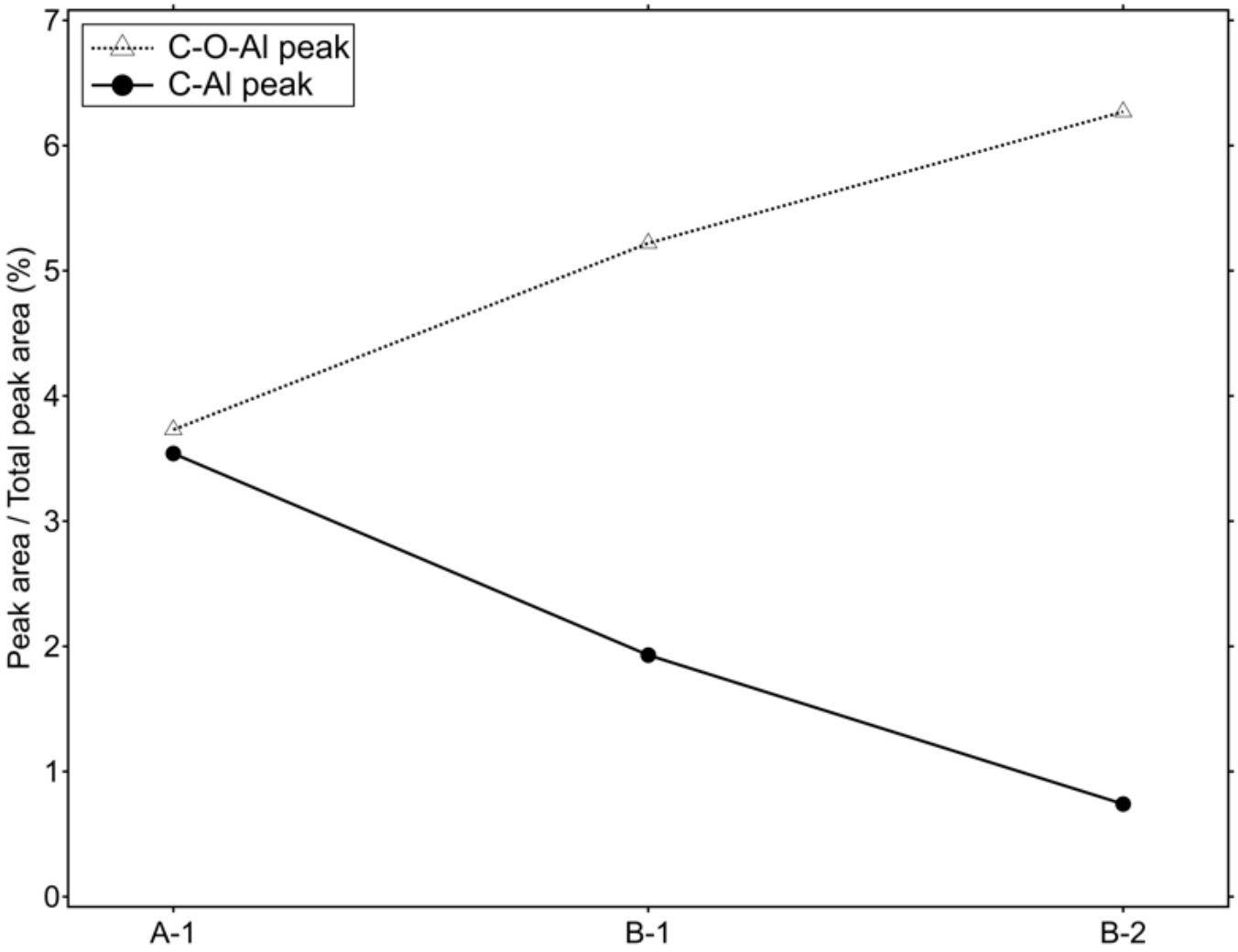

Figure 10

Ratio of C-O-Al and C-Al peak area over the total peak area.